# Integration of the Global Water and Lake Sectors within the ISIMIP framework through scaling of streamflow inputs to lakes

Ana I. Ayala[1], José L. Hinostroza[2], Daniel Mercado-Bettín[3], Rafael Marcé[3], Simon N. Gosling[4], Donald C. Pierson[1], Sebastian Sobek[1]

[1]Limnology Unit, Department of Ecology and Genetics, Uppsala University, Uppsala, Sweden.
[2]Faculty of Civil Engineering, National University of Engineering, Lima, Perú.
[3]Centre for Advanced Studies, National Spanish Research Council (CEAB-CSIC), Blanes, Spain.
[4]School of Geography, University of Nottingham, Nottingham, United Kingdom.

*Correspondence to*: Ana I. Ayala (isabel.ayala.zamora@ebc.uu.se)

**Abstract.** Climate change impacts both lakes and their surrounding catchments, leading to altered discharge and nutrient loading patterns from catchments to lakes, as well as modified thermal stratification and mixing dynamics within lakes. These alterations affect biogeochemical processes and water quality in lakes. Coupled catchment-lake modeling provides both a holistic evaluation of the effects of climate change on lakes and a framework for explicitly assessing the importance of how catchments effect lakes. The Inter-Sectoral Impact Model Intercomparison Project (ISIMIP) provides a framework for projecting the impacts of climate change across multiple sectors (e.g. water, lakes, energy, health) of the Earth System consistently, enabling integrated cross-sectoral assessments. However, climate impacts on lake dynamics are modeled in ISIMIP without consideration of the links between lakes and the surrounding catchments. This is a significant limitation, as it restricts assessments to only the direct impacts of climate change on lakes, overlooking the critical interactions between lakes and their catchment areas. In this study, we establish the first dynamic connection between the Global Water and Lake Sectors in ISIMIP, achieved by scaling the gridded modeled outputs of water fluxes from the Global Water Sector to the catchments of the representative lakes of the Lake Sector. The streamflow to the representative lake of each grid cell, as defined by the ISIMIP Global Lake Sector, was calculated based on runoff proportional to the catchment area of each representative lake. If the lake surface area was larger than the grid cell area, water from upstream grid cells was included as the corresponding proportion of river discharge. The methodology was applied to 70 lakes across Sweden covering a wide range of sizes, hydrological settings and catchment characteristics. The estimated streamflow was validated against both the streamflow outputs from the hydrological model HYPE and observed data. The comparison demonstrated good agreement in terms of long-term streamflow mean and seasonal pattern, indicating that the proposed approach is capable of producing reliable streamflow estimates without requiring high-resolution local models. This estimated streamflow, representing water flow into lakes, will provide a valuable dataset for the scientific community within the ISIMIP Lake Sector supporting hydrological and water quality modeling efforts aimed at understanding the impacts of climate change on lakes.

## 1 Introduction

Climate change impacts both catchments and lakes in distinct yet interconnected ways, influencing their physical, chemical, and biological processes. On one hand, alteration of precipitation patterns and increases in air temperature lead to hydrological changes in catchments. At high latitudes, winter precipitation increases and increased air temperature shift precipitation from
35 snow to rain, reducing snowpack and leading to earlier spring snowmelt, resulting in greater streamflow and nutrients loading during this period (Jiménez-Navarro et al., 2021). Higher air temperatures also lead to greater evapotranspiration rates (Donnelly et al., 2017; Liu et al., 2021), which reduce streamflow and increase nutrient concentration during the summer. Extreme precipitation leads to increased nutrient loading in both wet and dry areas, through increased runoff in wet areas, and soil erosion and the mobilization of nutrients trapped in soils in dry areas (Costa et al., 2023). On the other hand, increases in
40 air temperature result in increased lake surface water temperature (O'Reilly et al., 2015) with stronger thermal stratification and reduced mixing (Kraemer et al., 2015), earlier onset of summer stratification (Magee and Wu, 2017; Moras et al., 2019) and shorter ice-cover periods (Sharma et al., 2019, 2021). Warmer water temperatures promote the growth of cyanobacteria, leading to the formation of harmful algal blooms (Paerl and Huisman, 2008; Huisman et al., 2018).

Stronger lake stability and longer duration of thermal stratification lead to hypolimnetic oxygen depletion (Jane et al., 2021;
45 Jansen et al., 2024), resulting in increased internal loading (North et al., 2014) and greenhouse gas emission (Marotta et al., 2014; Vachon et al., 2019; Jansen et al., 2022). Earlier ice loss leads to greater heat loss due to increased evaporation rates (Wang et al., 2018; Li et al., 2022). Nonetheless, climate change affects lake ecosystems through a complex and dynamic interplay of catchment loading and lake-internal processes. For instance, changes in the timing of streamflow and lake ice-off lead to earlier onset of spring phytoplankton blooms (Gronchi et al., 2021; Mesman et al., 2024). Lake water level fluctuations
50 caused by dry conditions during periods of strong stratification limit vertical mixing, which contributes to pronounced hypolimnetic hypoxia. This hypoxia is exacerbated by intense precipitation events that subsequently reduce oxygen concentrations in the water column and lower the pH level (Saber et al., 2020).

The integration of catchments and lakes using coupled dynamic models provides valuable insights into the functioning of lake ecosystems and the impacts of climate change, for example to understand how changes in the surrounding catchment area,
55 within the lake itself, and their interactions affect the lake's dynamics. Additionally, this modeling approach can inform the development of adaptation and mitigation strategies.

The Inter-Sectoral Impact Model Intercomparison Project (ISIMIP, https://www.isimip.org) is a collaborative framework for assessing the impacts of climate change across temporal and spatial scales, by integrating climate models, impact models, and direct human forcing data to provide insights into climate change risk and inform potential adaptation and mitigation strategies.
60 ISIMIP is organized into multiple sectors that represent natural and human components of the Earth system, that are both regulators of climate and vulnerable to its changes, including agriculture, forests, fisheries and marine ecosystems, water, lakes, energy, health, among others. To ensure consistency in impact modeling within and across sectors, ISIMIP provides a common set of climate-related and direct human forcing data, and along with a modeling protocol sets up standardized

experiments, spanning pre-industrial and historical periods and future projections (Frieler et al., 2024). This framework enables multi-model impact simulations within sectors, enhancing the robustness and reliability of model projections (Rosenzweig et al., 2017) and quantifying the sources of uncertainty in the projections (Krysanova et al., 2017; La Fuente et al., 2024a; Jones et al., 2025). In addition, it enables cross-sectoral assessment of climate change impacts (Lange et al., 2020; Vanderkelen et al., 2020). However, cross-sectoral integration remains a challenge within ISIMIP, which limits the potential for capturing complex interdependencies, cascading effects, and feedback loops between sectors. For example, simulations from the Water Sector and the Lake Sector are at present not connected to each other.

The ISIMIP Lake Sector modeling has focused on lake physics and thermal dynamics, including changes in water temperature (Ayala et al., 2020, 2023b), loss of ice cover (Grant et al., 2021; Sharma et al., 2021), stratification phenology (Woolway et al., 2021b, 2022b), alterations in mixing regimes (Woolway and Merchant, 2019), occurrence of lake heatwaves (Woolway et al., 2021a, 2022a), shifts in lake thermal regions (Maberly et al., 2020), heat uptake (Vanderkelen et al., 2020), surface heat fluxes (Ayala et al., 2023a) and lake evaporation (La Fuente et al., 2022, 2024b, a). Hydrodynamic lake model simulations were performed under the premise that lake water temperature variation results solely from the exchange of energy between the lake surface and the atmosphere (Golub et al., 2022). However, the advective fluxes are particularly relevant for water bodies with significant water level fluctuations and rapid water exchange, such as reservoirs or lakes with short residence times. Fenocchi et al. (2017) showed that in a deep subalpine lake a hydrodynamic lake model, when excluding through-flows, required unrealistically low light extinction coefficient to reproduce temperatures in the epilimnion and upper metalimnion. In contrast, incorporating through-flows together with a realistic light extinction coefficient improved the accuracy of temperature predictions in the lower metalimnion and upper hypolimnion. Råman Vinnå et al. (2018) investigated the tributary influences on lakes in a study of Lake Biel and Lake Geneva and revealed that seasonal variations in river discharge and temperature significantly affect lake warming and stratification, underscoring the importance of hydrologic inputs in thermal lake modeling.

Integrating the ISIMIP Water Sector and Lake Sector, incorporating hydrologic model outputs into lake model simulations, can improve the accuracy of thermal stratification and mixing dynamics in lakes and the assessment of climate change impacts. It will also provide the basis for more complex simulations of lake biogeochemistry and water quality parameters, for which inputs from the upstream catchment are paramount.

The Global Water Sector in ISIMIP (Telteu et al., 2021; Müller Schmied et al., 2024a) focuses on assessing the impacts of climate change on water fluxes, including discharge, total (surface + subsurface) runoff and evapotranspiration, among other hydrological variables, with a global grid resolution of 0.5° by 0.5°. The Global Lake Sector in ISIMIP has assigned one representative lake to each 0.5° grid cell, which simplifies the complexity of modeling all lakes globally. This ensures computational feasibility while capturing variations in lake responses to climate change, and provides a practical way to include lake-specific dynamics in a global-scale assessment.

Here, gridded water fluxes simulated by WaterGAP 2 following the ISIMIP phase 3a protocol were scaled to match the individual lake catchment areas for estimating the streamflow of 71 lake catchments across Sweden. The catchment-scale streamflow simulations were then validated against both the streamflow outputs of the hydrological model HYPE, which

simulates hydrological processes at the catchment scale, and observed data. The use of HYPE provides an additional benchmark, with its outputs serving as an established reference dataset where observational data are limited.

## 2. Material and methods

### 2.1. Gridded simulations of streamflow from the ISIMIP3a Global Water Sector

Water Global Assessment and Prognosis (WaterGAP) is a process-based hydrological model used for quantifying water resources and water use on a global scale (Alcamo et al., 2003; Döll et al., 2003). WaterGAP 2 consists of three major components, the global water use model, the linking model GroundWater-SurfaceWater USE (GWSWUSE) and the WaterGAP Global Hydrology Model (WGHM) (Müller Schmied et al., 2021). The global water use model distinguishes five water use sectors, i.e., irrigation, livestock, domestic, manufacturing and cooling of thermal power plants, quantifying both consumptive waters use and water withdrawals. The linking model GWSWUSE computes the fractions of water withdrawals and consumptive use for all five sectors, distinguishing whether the water is sourced from groundwater or surface water bodies, such as lakes, reservoirs and rivers. The WGHM computes water flows (fast surface and sub-surface runoff, groundwater recharge, evapotranspiration and river discharge) and storage across ten compartments. The vertical water balance covers the canopy, snow and soil, while the lateral water balance includes groundwater, lakes, reservoirs, wetlands and rivers.

The computational grid of WaterGAP 2 is based on the CRU land-sea mask (Mitchell & Jones, 2005), which covers the global continental area with the exception of Antarctica, comprising 67420 grid cells of 0.5° longitude x 0.5° latitude, and the upstream–downstream relations among the grid cells are defined by the drainage direction map DDM30 (Döll and Lehner, 2002). Model input includes climate data, land use and land cover data, soil characteristics, location and extent of surface water bodies (lakes, wetlands, dams and reservoirs), the river routine network (basins, flow direction and slopes) and human water use data. Although WaterGAP 2 includes the representation of lakes in its simulations (Müller Schmied et al., 2021), accounting for their role in storing water, evaporation and downstream release, it does not explicitly resolve the amount of water flowing into individual lakes from upstream locations. Instead, the model estimates water flows at the grid cell level, without disaggregating them to accurately capture inflow to specific lakes. As a result, it lacks the spatial resolution needed to track lake specific inflow in details.

WaterGAP 2.2e contributed to ISIMIP3a, specifically in the Global Water Sector (Müller Schmied et al., 2023), following the ISIMIP3a simulation protocol. The protocol (https://protocol.isimip.org) outlines the required experiments, input data sets and output variables necessary for participation. Input data (climate forcing, socioeconomic forcing and static geographic information) and impact model outputs are available at https://data.isimip.org.

Here, we focused on the standard model evaluation experiment *obsclim_histsoc_default* (Frieler et al., 2024), which is based on the observed climate-related forcing *obsclim* from the GSWP3-W5E5 climate forcing dataset (Kim, 2017; Cucchi et al., 2020; Lange et al., 2021) combined with the direct human forcing (e.g. land use and land cover changes and water

management) *histsoc*. This experiment reproduces observed long-term changes in hydrological change and water use from
1901 to 2019. The impact model WaterGAP 2.2e ([https://www.isimip.org/impactmodels](https://www.isimip.org/impactmodels)) provided monthly total (surface + subsurface) runoff, $q_{tot}$ [kg m$^{-2}$ s$^{-1}$], groundwater runoff, $q_g$ [kg m$^{-2}$ s$^{-1}$], and discharge, *dis* [m$^{-3}$ s$^{-1}$]. Note that, $q_{tot}$ and $q_g$ represent the runoff produced within a grid cell, which includes both surface and subsurface, and groundwater components. Meanwhile, *dis* represent the routed (i.e. via river channels) discharge at a given grid cell, which includes the runoff generated within that grid cell plus the contribution from upstream grid cells. This means *dis* accounts for both locally generated runoff and the cumulative flow from upstream grid cells, which results in the total discharge flowing downstream.

## 2.2 Representative lakes in the ISIMIP3a Global Lake Sector

In the ISIMIP3a Global Lake Sector, each 0.5°grid cell was assigned a representative lake sourced from the HydroLAKES database (Messager et al., 2016). The selection of the representative lake for each grid cell was based on the location of the lake centroid. When multiple lakes were present within a grid cell, the representative lake was selected based on the lake depth corresponding to the weighted median of all lakes within the respective grid cell (weighted by the area of the lake) (Golub et al., 2022), resulting in a total of 41449 representative lakes. The catchment areas for these representative lakes were derived from the HydroLAKES database (Messager et al., 2016).

## 2.3 Study sites

Our study sites comprised 70 lakes across Sweden, which correspond to representative lakes from the ISIMIP3a Global Lake Sector (Figure 1). The site selection included lakes with a wide range of surface areas and catchments of varying sizes (Table S1). Additionally, the lakes were located in different physiographic regions, ranging from agriculturally dominated lowland areas in the south to boreal and subarctic regions in the north. Accordingly, the surface area, $A_{lake}$, ranged from 0.34 to 5486 km$^2$, with mean and median values of 176.26 and 23.25 km$^2$, respectively. The catchment area, $A_{catchment}$, varied from 101 to 48421 km$^2$, with mean and median values of 4542 and 1698.35 km$^2$, respectively. The ratio between $A_{catchment}$ and $A_{lake}$ ranged from 3.37 to 14962. The mean and median ratio $A_{catchment}$ to $A_{lake}$ were 386.99 and 48.30.
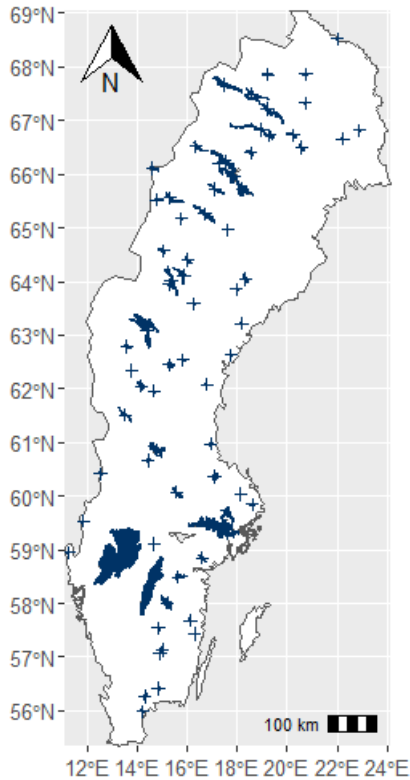
**Figure 1. Study sites, marked either as crosses (small lakes) or blue lake shapes (large lakes).**

### 2.4 Scaling streamflow from 0.5°grid cells to catchment scale

155  To estimate the streamflow into representative lakes, we applied a scaling approach that adjusts grid-based hydrological outputs to the actual catchment area of the lakes. The method is structured into three approaches, depending on the size of the catchment relative to the grid cell area where the lake centroid is located:

- Approach I.a: Applied when the catchment area is smaller than or equal to the area of the grid cell containing the lake centroid.

160  - Approach I.b: Applied when the catchment area spans multiple grid cells.

- Approach II: Applied for large lakes where the lake area spans multiple grid cells.

The water flow into the representative lake was calculated based on total (surface + subsurface) runoff, $q_{tot}$ [m s$^{-1}$], and groundwater runoff, $q_g$ [m s$^{-1}$], in proportion to the catchment area of the representative lake, $A_{catchment}$ [m$^2$] (Figure 2). The catchment was delineated using upstream grid cells based on the flow direction. The grid cells contributing water flow towards

165  the lake were classified into levels: grid cells partially occupied by the lake correspond to level 0; each level 0 grid cell received water flow from one or more of its eight neighbouring grid cells, which were classified as level 1; this process continued, with the neighbouring grid cells of level 1 classified as level 2, etc (Figure 4). The ratio ($N$) of catchment area, $A_{catchment}$, to grid cell

area (grid cell area where the lake centroid is located), $A_{grid}$, indicated how many grids cell occupied the catchment and determines the number of grid cells to be counted in the water flow calculation (Figure 2).
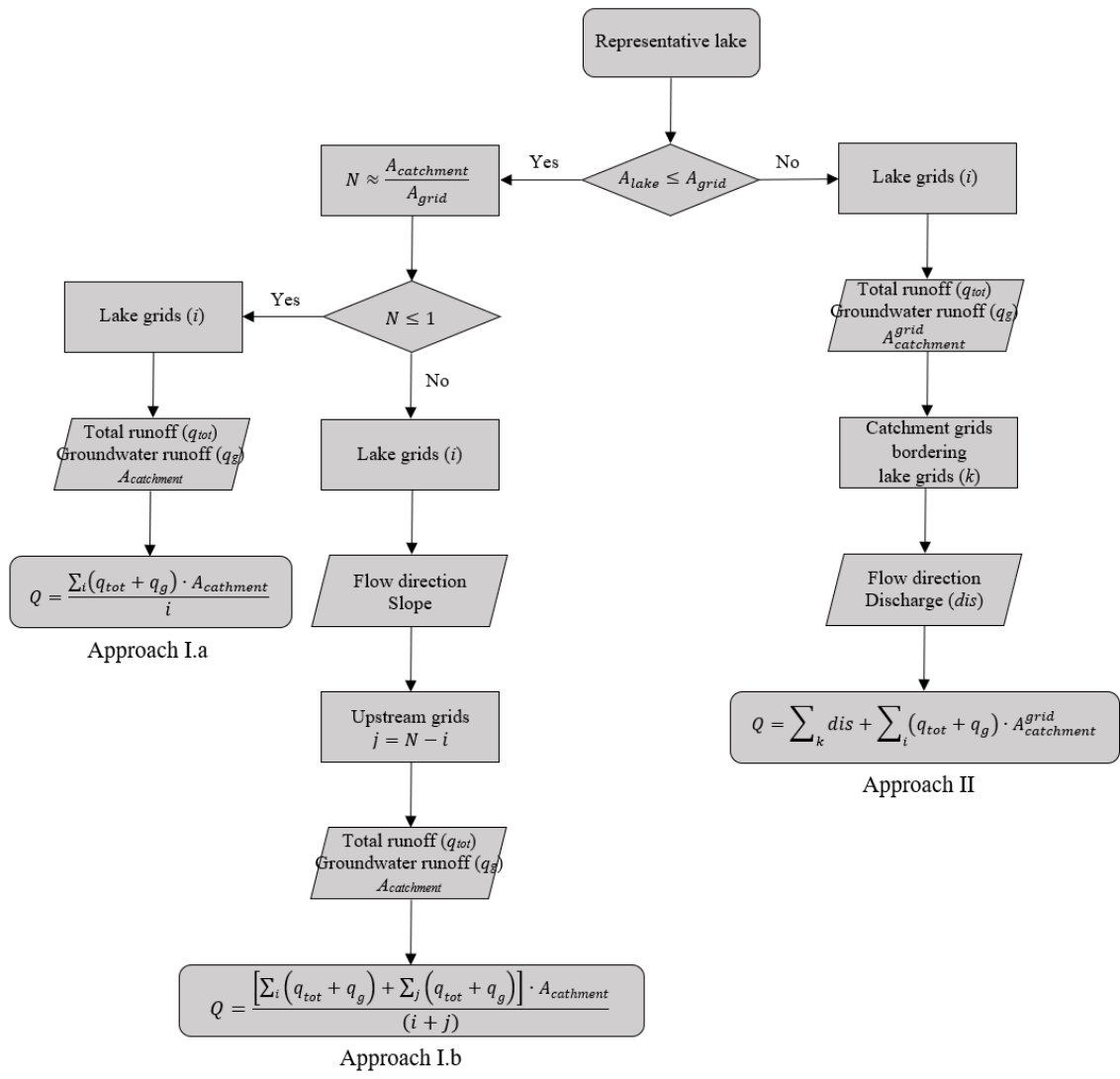
170

**Figure 2. Workflow for estimating streamflow to lakes by scaling grid cells to catchment scale.**

For $N \leq 1$ (Approach I.a), the catchment area was smaller or equal to the grid cell area where the lake centroid was located. Note that, $N$ was rounded down to the nearest integer number, meaning the catchment area can be slightly greater than the lake grid cell area. Only grid cells partially occupied by the lake (grid cells of level 0) were counted ($i$) (Figures 2 and 3). For

175 example, lake 12247 (Figure 3) had an $A_{lake}$ of 22.46 km² and partially occupied 2 grid cells. $A_{catchment}$ was 1662 km², which was slighter greater than the $A_{grid}$ of the grid cell where the lake centroid was located, which was 1415.32 km², resulting in a $N$ equal to 1. Therefore, the grid cells occupied by the lake (grid cells of level 0) were included in the count ($i = 2$).
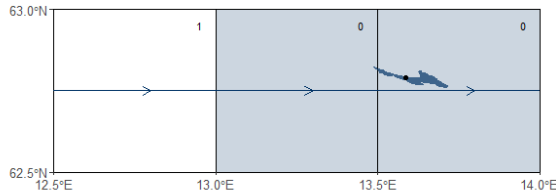
**Figure 3. Catchment-lake scheme for lake 12247 ($A_{lake}$ = 22.46 km², $A_{catchment}$ = 1662 km², $A_{grid}$ = 1415 km² and $N$ = 1). The dot denotes the lake centroid, respectively. The arrows indicate the flow direction, and the numbers indicate the grid cell levels. The blue-shaded grid cells represent those selected for the streamflow estimation, according to the workflow (Figure 2).**

However, for N > 1 (Approach I.b), the catchment occupied multiple grid cells. As a result, both grid cells partially occupied by the lake and upstream grid cells were counted. In addition to the grid cells of level 0 ($i$), the number of upstream grid cells, $j = N - i$, were counted by levels, selecting as many grid cells as indicated by $j$. This ensures that the total contributing area, represented by $i + j$ grid cells, approximates the scaled catchment size $N$. Once all level 1 grid cells have been counted, we proceed to the next level, continuing the process until $j$ grid cells have been counted (Figure 4). If not all grid cells at the same level can be counted (when the available grid cells at a given level exceed $j$ or the remaining $j$), those with the steepest slope were prioritized (Figure 2). For example, lake 11693 (Figure 4) has an $A_{catchment}$ of 11316 km², while the grid cell where the lake centroid is located has an $A_{grid}$ of 1220.18 km², resulting in $N$ = 9. Of the 9 grid cells counted, 2 corresponded to level 0 ($i$ = 2), representing grid cells partially occupied by the lake. For the upstream grid cells ($j$ = 7), 2 of the 7 grid cells corresponded to level 1, 2 to level 2, and 3 to level 3.
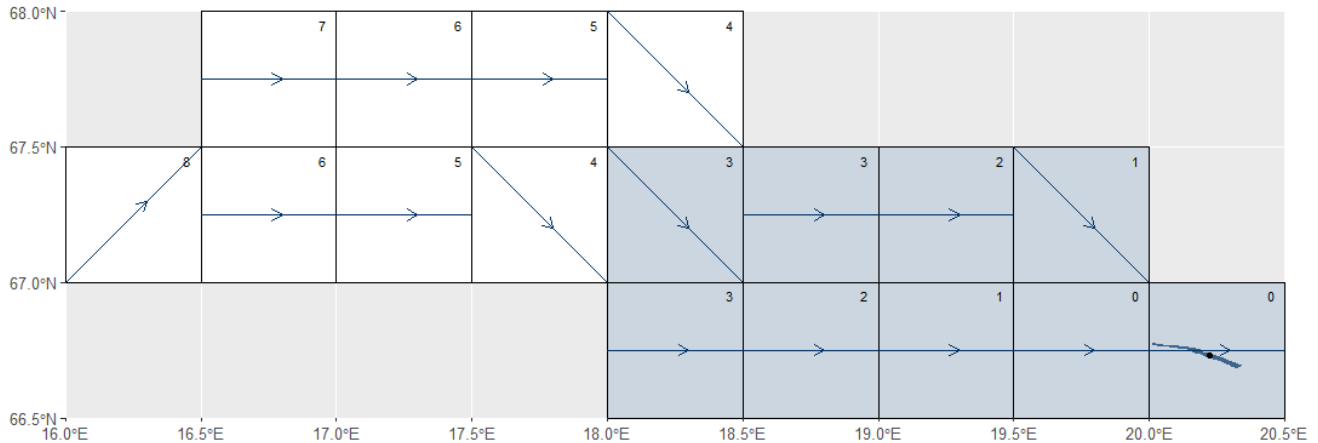
**Figure 4. Catchment-lake scheme for lake 11693 ($A_{lake}$ = 21.05 km², $A_{catchment}$ = 11316 km², $A_{grid}$ = 1220 km² and $N$ = 9). The dot denotes the lake centroid and the pour point, respectively. The arrows indicate the flow direction, and the numbers indicate the grid cell levels. The blue-shaded grid cells represent those selected for the streamflow estimation, according to the workflow (Figure 2).**

For large lakes where the surface area, $A_{lake}$, exceeded the $A_{grid}$ (Approach II) the water flow from upstream grid cells was included as river discharge, $dis$ [m$^3$ s$^{-1}$], at the catchment grid cells bordering the lake grid cells ($k$, grid cells classified as level 1), in addition to $q_{tot}$ [m s$^{-1}$] and $q_g$ [m s$^{-1}$] proportional to the land area of the grid cells partially occupied by the lake ($i$, grid cells classified as level 0), $A_{catchment}^{grid}$ [m$^2$] (Figures 2 and 5). The inclusion of $dis$ was necessary because, in large lakes, a

200    significant portion of inflow enters not as diffuse runoff from adjacent land areas, but as a concentrated river discharge delivered through from upstream flow paths or tributaries. Lake grid cells ($i$) that did not flow into the lake, such as the grid cell where the outlet of the catchment is located or grid cells acting as sinks (usually to the ocean), were excluded. For example, lake Vänern – 105 (Figure 5) spans 12 grid cells ($i$) with an additional 18 upstream grid cells. Of the $i$ lake grid cells, the pour point grid cell was excluded because it was flowing out of the lake. Streamflow was calculated as the product of $q_{tot}+q_g$ and

205    $A_{catchment}^{grid}$ for each of the remaining 11 grid cells at level 0 ($i = 11$). Additionally, the $dis$ contribution from 7 bordering grid cells within the 18 upstream cells ($k = 7$, level 1 grid cells) was included.
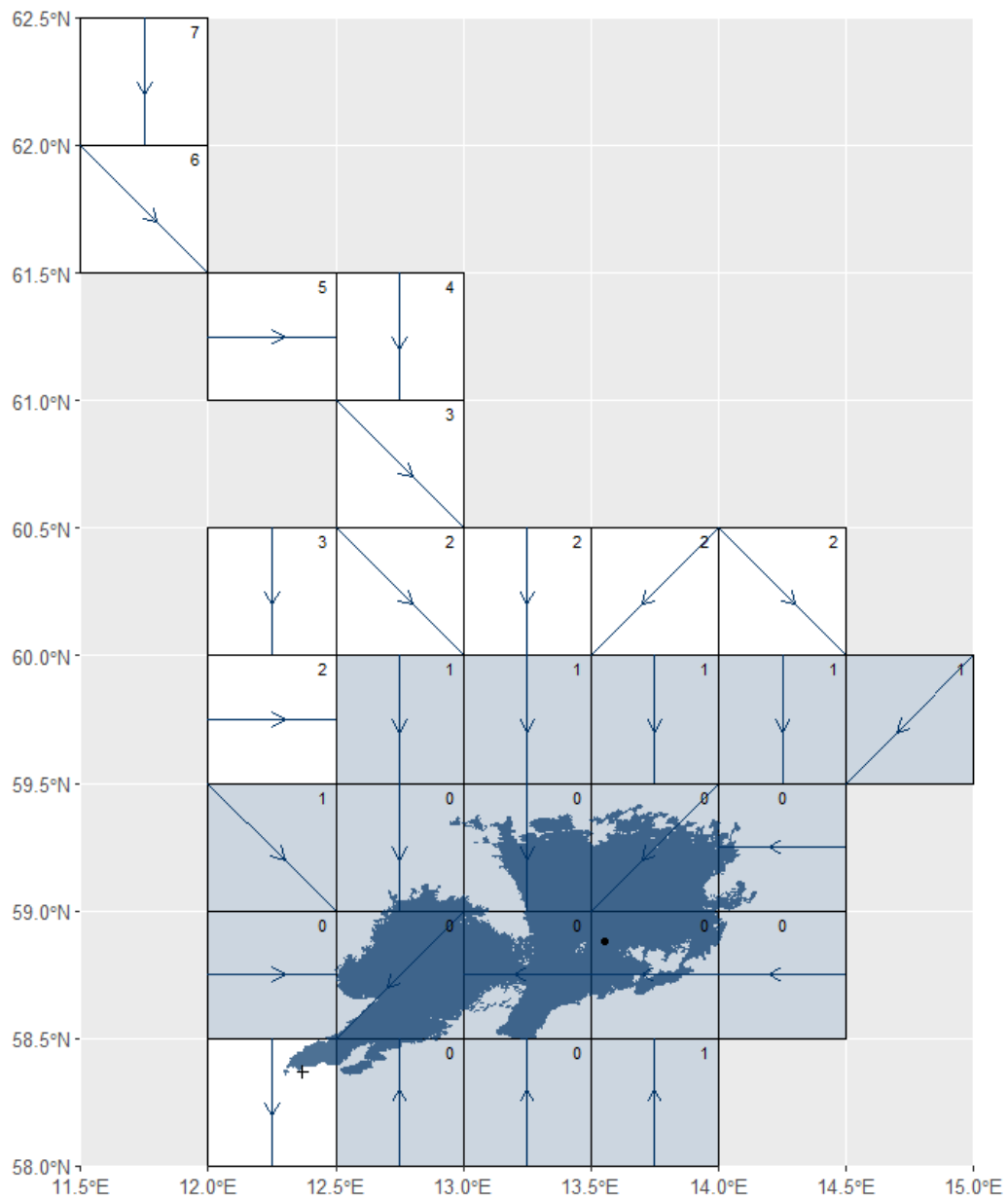
**Figure 5. Catchment-lake scheme for lake Vänern – 105 ($A_{lake}$ = 5486 km², $A_{catchment}$ = 48421 km² and $A_{grid}$ = 1604 km²). The dot and cross denote the lake centroid and the pour point, respectively. The arrows indicate the flow direction, and the numbers indicate the grid cell levels. The blue-shaded grid cells represent those selected for the streamflow estimation, according to the workflow (Figure 2).**

## 2.5 Validation of streamflow at catchment scale

Historical simulations of daily river discharge of the hydrological model HYPE (Hydrological Predictions for the Environment; Lindström et al., 2010), which is used operationally and was developed by Swedish Meteorological and Hydrological Institute

(SMHI), are openly available for 35447 sub-catchments across Europe over a 30-year period (1981-2010) (Donnelly et al., 2016; https://hypeweb.smhi.se/explore-water/historical%20data/europe-time-series). The HYPE discharge simulations (hereafter referred to as the reference dataset) were used to evaluate the performance of the developed methodology for scaling streamflow from grid cells to catchment scale.

The HYPE model was forced with ERA5 reanalysis climate data (Donnelly et al., 2016), ensuring that the simulations provided an independent dataset for validation. Daily HYPE outputs were averaged to produce monthly and annual discharge values, which were then compared to our monthly estimations and derived annual averages calculated from the monthly values over the common period (1981-2010) across 70 study sites.

Monthly and annual averages derived from daily observed river discharge at stations downstream of 10 lakes, which are also representative lakes within the ISIMIP Global Lake Sector (lakes: Vänern – 105, Vättern – 104, Mälaren – 102, Siljan – 1150, lake 12423, lake 12791, Erken – 12809, Roxen – 12965, lake 142240, and Hasselasjön – 152977), available from the Swedish Meteorological and Hydrology Agency (SMHI; https://www.smhi.se/data), were also compared with the corresponding monthly and annual average simulated and reference streamflow. Although the observed data represent discharge downstream of the lakes (lake outflows), while the simulations estimate lake inflows, we assume that the atmospheric water exchange (precipitation and evaporation) over the lake surfaces in Sweden are relatively minor compared to total inflow and outflow volumes, particularly at monthly and annual timescales (Text S1).

Performance was assessed using the Kling-Gupta efficiency, $KGE$, metric. $KGE$ decomposes model performance into three aspects: the linear correlation coefficient, $KGE_r$, the bias ratio, $KGE_b$, and the variability ratio, $KGE_g$, which assess the model's ability to reproduce timing, mean and variability, respectively (Gupta et al., 2009; Kling et al., 2012).

$$KGE = 1 - \sqrt{(KGE_r - 1)^2 + (KGE_b - 1)^2 + \left(KGE_g - 1\right)^2} \tag{1}$$

$$KGE_b = \frac{\mu_{sim}}{\mu_{obs}} \tag{2}$$

$$KGE_g = \frac{CV_{sim}}{CV_{obs}} = \frac{\frac{\sigma_{sim}}{\mu_{sim}}}{\frac{\sigma_{obs}}{\mu_{obs}}} \tag{3}$$

where $\mu_{sim}$ and $\mu_{obs}$ are simulated and observed mean, and $\sigma_{sim}$ and $\sigma_{obs}$ are simulated and observed standard deviation. All three metrics have an optimum value of 1. The three individual metrics are combined into an overall model performance, $KGE$, by calculating the Euclidean distance from the ideal point. The error term is subtracted from unity to constrain the metric between 1 (perfect agreement) and –∞. Based on Knoben et al. (2019), $KGE$ is interpreted as: $KGE$=1 perfect agreement, 0.75≤$KGE$<1 very good performance, 0.50≤$KGE$<0.75 good performance, 0.25≤$KGE$<0.50 acceptable performance and $KGE$<0.25 poor performance.

Additional goodness-of-fit metrics for comparing reference and simulated values, such as the Mean Bias Error ($MBE$), Root Mean Square Error ($RMSE$), Normalized Root Mean Square Error ($NRMSE$) and Nash-Sutcliffe Efficiency ($NSE$; Nash & Sutcliffe, 1970), can be found in the Supplementary Material.

## 3. Results

The performance of the scaled streamflow simulations from grid cells to the catchment scale (hereafter referred to as simulations) was evaluated for monthly time series over the period 1981-2010 across 70 study sites (Figure 6A; Table S2). The average Kling-Gupta efficiency, $KGE$, was 0.59±0.18 (mean ± standard deviation), with individual values ranging from -
250 0.07 to 0.86. For all study sites, the $KGE$ exceeded -0.41, indicating that the simulated streamflow provided added value compared to simple prediction based on the long-term mean streamflow.

To better diagnose performance, $KGE$ was decomposed into its three components: correlation ($KGE_r$), bias ($KGE_b$) and variability ($KGE_g$). The average $KGE_r$ was 0.79±0.08, suggesting generally strong agreement between reference and simulated streamflow timing. A total of 52 out of 70 sites (74 %) exhibited a $KGE_r$ greater than 0.75, reflecting very good representation
255 of seasonal and interannual flow dynamics. The bias component, $KGE_b$, averaged 1.06±0.30, was close to the optimal value of 1, indicating that the overall volume of streamflow was, on average, well captured. However the relatively high standard deviation highlights substantial variability in bias among the study sites. Only 39 study sites (56%) had a $KGE_b$ within the range of 0.75 to 1.25, indicating that for a significant number of study sites, deviations in simulated streamflow volumes were a key source of reduced performance. The variability component, $KGE_g$, averaged 0.88±0.22, indicating generally very good
260 representation of streamflow variability, though with some underestimation of streamflow. Similar to $KGE_r$, 52 sites (72%) had $KGE_g$ values within the range of 0.75 to 1.25. In summary, the simulations demonstrated generally very good performance in reproducing time and variability of monthly streamflow across study sites. However, discrepancies in the magnitude of the simulated streamflow, reflected in the higher variability of $KGE_b$, where the bias component more frequently deviated from its optimal range compared to the correlation and variability components (Figure 6A).

265 The inter-annual variability of streamflow was assessed by comparing the simulated and reference annual average streamflow (Table S2; Figure S2). The average values of the $KGE$ components were $KGE_r$ of 0.77±0.14, $KGE_b$ of 1.06±0.30, $KGE_g$ of 1.06±0.31, indicating an overall very good performance in responding differently to wet and dry years. The relatively high $KGE_r$ suggest that the simulated streamflow timing was very well captured. However, the standard deviations of both $KGE_b$ and $KGE_g$ were relatively large, reflecting considerable variability in the ability to simulate annual streamflow volumes and
270 variability. While the mean values of $KGE_b$ and $KGE_g$ were close to the optimal value of 1, these high standard deviations indicate that performance differed substantially among study sites, with some ties showing over- or underestimation of interannual streamflow characteristics. The combined $KGE$ for interannual streamflow was 0.54±0.23, which is slightly lower but comparable to the $KGE$ (0.59±0.18) for monthly streamflow, suggesting that the model maintained reasonable skill across both temporal scales.

275 Performance was further analysed based on the streamflow scaling approach. Of the 70 study sites, 68 were analysed using Approach I ($A_{lake} \leq A_{grid}$), with 39 study sites following Approach I.a ($N \leq 1$) and 29 study sites following Approach I.b ($N >$ 1). The average $KGE$ was 0.56±0.15 for Approach I.a and 0.60±0.21 for Approach I.b, indicating similar performance across these two subcategories. In 5 of the Approach I.b study sites, an additional comparison was made between counting all grid

cells at the last level versus only those with the steepest slope. In both cases, the performance was acceptable, and the differences between *KGE* and its components were marginal. When all grid cells were counting at the last level, the *KGE* was 0.49±0.31, with *KGE$_r$* of 0.76±0.05, *KGE$_b$* of 0.87±0.17, *KGE$_g$* of 1.23±0.49; when only the steepest grid cells were counted the KGE was 0.48±0.31, with *KGE$_r$* of 0.74±0.07, *KGE$_b$* of 0.85±0.15, *KGE$_g$* of 1.22±0.49). These small differences suggest that the method is robust to the choice of how grid cells are selected at the last level.

The Approach II ($A_{lake} > A_{grid}$) was applied to the two largest lakes in this study: Vänern (105) and Vättern (104), the performance was very good in both Vänern and Vättern (Figure 6), with a *KGE* of 0.77 (*KGE$_r$* of 0.85, *KGE$_b$* of 0.97, *KGE$_g$* of 1.17) and 0.79 (*KGE$_r$* of 0.79, *KGE$_b$* of 0.97, *KGE$_g$* of 1.00), respectively. Lake Mälaren (102), the third largest lake in Sweden, extends over 9 grid cells (Figure S1); however, its $A_{lake}$ (of 1083 km$^2$) does not exceed the $A_{grid}$ of 1580 km$^2$ due to its irregular and branched shape. Scaling streamflow Approach I.b ($A_{lake} \leq A_{grid}$ for $N > 1$) and Approach II ($A_{lake} > A_{grid}$) were tested (Figure 2). For Approach I.b, simulated streamflow showed good performance at the seasonal scale, with *KGE* of 0.71 (*KGE$_r$* of 0.72, *KGE$_b$* of 1.04, *KGE$_g$* of 1.06); however, errors in reproducing the timing of flow reduced the overall performance. In Approach II, the simulated seasonal streamflow was less accurate, with a *KGE* of 0.47 (*KGE$_r$* of 0.52, *KGE$_b$* of 0.98 and *KGE$_g$* of 0.80). The errors were caused by either a reduced ability to accurately reproduce the timing of flow increases and decreases; and an underestimation of the magnitude of the variability, although it was still acceptable.
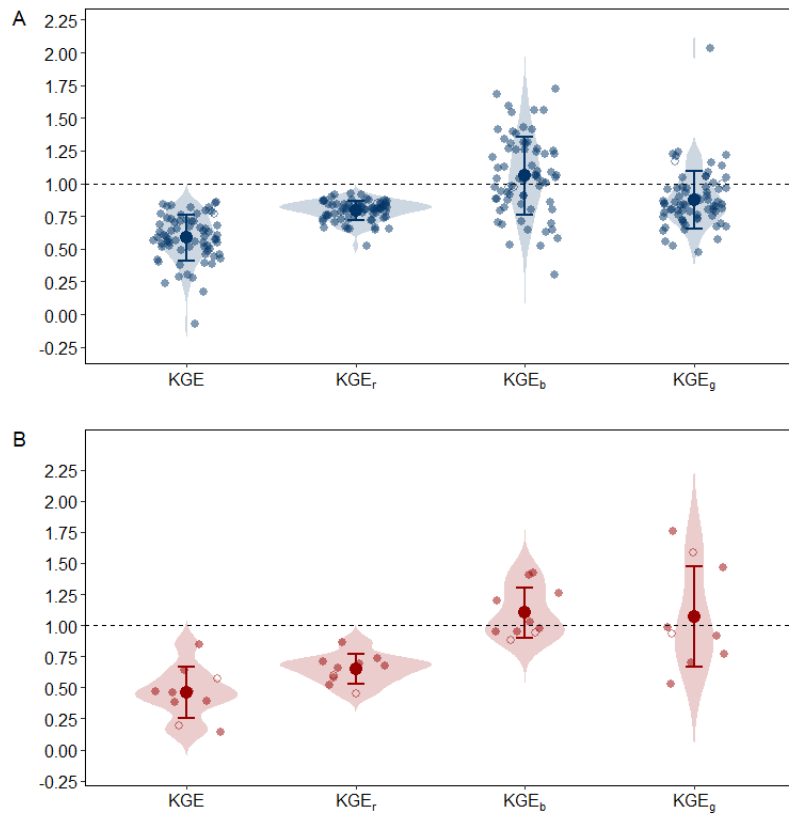
**Figure 6. Kling-Gupta efficiency (*KGE*)and its components, timing (*KGEr*), bias (*KGEb*) and variability (*KGEg*), when comparing monthly simulations of scaled streamflow with reference data from the HYPE model (A) and observed data (B) of streamflow. Filled dots correspond to study sites where $A_{lake} \leq A_{grid}$ (approach I) and unfilled dots corresponds to study sites where $A_{lake} > A_{grid}$ (approach II). The horizontal dashed line marks where *KGE* and its components equal 1, representing a perfect match**

In addition, the performance of simulated streamflow was assessed by comparing simulations with observations for 10 study sites, which are both representative lakes in the ISMIP3 Global Lake Sector and for where observations are available (Figure 6B; Table S3). At the seasonal scale, the average *KGE* was 0.46±0.21, with *KGEr* of 0.65±0.12, *KGEb* of 1.10±0.20, *KGEg* of 1.07±0.40. Overall performance was acceptable but was primarily limited by mismatches in flow timing. At the annual scale, the performance of the scaling streamflow from grid cells to catchment scale was good (*KGE* of 0.70±0.15, with *KGEr* of 0.85±0.05.83±0.05, *KGEb* of 1.10±0.20, *KGEg* of 0.98±0.20), indicating strong agreement in timing, bias and variability across study sites (Figure S2).

Finally, a further evaluation was conducted by comparing reference and observed streamflow for 9 study sites (note that the reference and observations datasets cover different time periods, which limited direct comparability in the 10 study sites for which observations were available) (Table S4). At the monthly scale, the average *KGE* was 0.44±0.44 (with *KGEr* of 0.65±0.23, *KGEb* of 1.12±0.34, *KGEg* of 1.13±0.46), indicating on average acceptable agreement with substantial inter-site differences. At the yearly scale, performance improved to *KGE* of 0.55±0.26 (with *KGEr* of 0.78±0.12, *KGEb* of 1.12±0.34, *KGEg* of 0.77±0.19). Overall, these results demonstrate that the scaling method provides added value, improving the simulations of streamflow compared with standard catchment-scale hydrological models.

We conclude that the overall performance of the scaled streamflow simulations matched satisfactorily to both reference (derived from the hydrological model HYPE) and observed streamflow (Figure 7; Figures S3-S11).
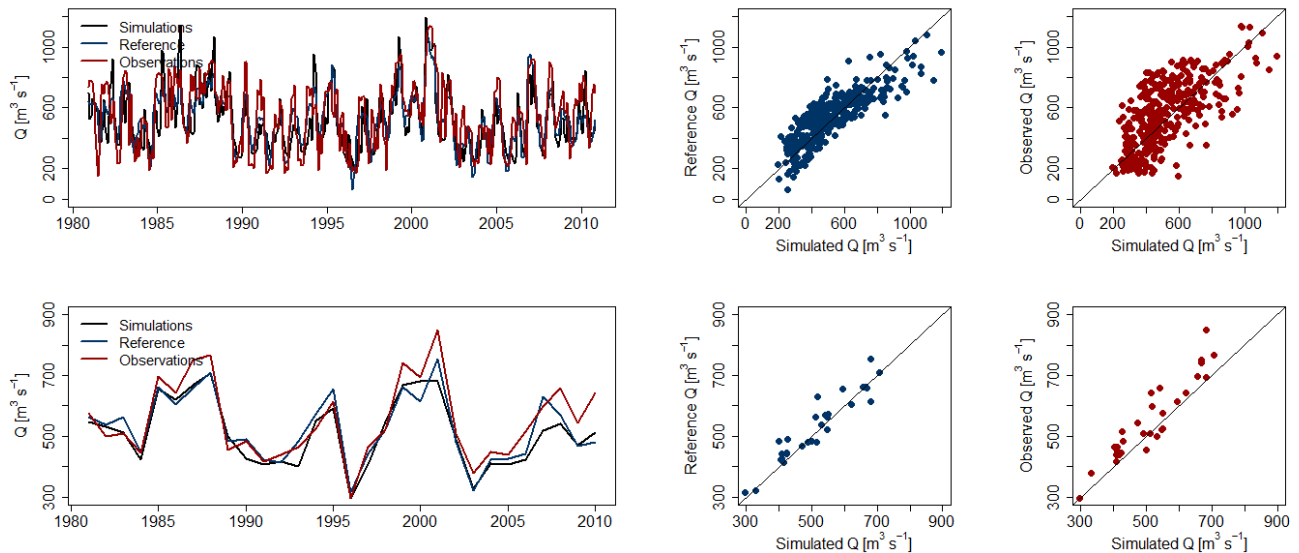
**Figure 7. Monthly (upper row) and annual (lower row) comparison of simulated (black), reference (blue) and observed (red) streamflow for lake Vänern (105) over a 30-year period (1981–2010).**

## 4. Discussion

This study demonstrates a scaling approach that reliably estimates streamflow to individual lakes from gridded streamflow data, showing strong agreement between simulations, reference data, and observations. The fit of our simulated scaled streamflow was acceptable regardless of temporal scale (monthly, Figure 6; annually, Figure S2), and geospatial configuration i.e. the location and size of the lake and its catchment, corresponding to the scaling Approaches I.a, I.b and II (Figure 6; Figure S2). The simulated scaled streamflow also fitted reference data as well as observations equally well (Figures 6-7; Figures S3-S11). These conclusions are based on the evaluation of the performance of scaled streamflow simulations across 70 study sites in Sweden, and the country's diverse landscape, which includes a wide range of lake sizes, catchment sizes and land covers, climate conditions and topography, thus providing a robust basis for assessing model performance. This diversity enhances the generalizability of the validation results across different hydrological settings. Further, Donnelly et al. (2016) demonstrated that Sweden has a well-established hydrological modeling framework, particularly through the HYPE (Hydrological Predictions for the Environment) model, which has been extensively applied and validated in the region, and which was used as a reference data source in this analysis. In addition, Sweden has long-term, high-resolution datasets for precipitation, temperature and streamflow, which are essential for ensuring robust hydrological simulations, making the HYPE model optimal for testing the accuracy of scaled streamflow simulations. We feel that the regionally focused nature of HYPE should provide an excellent comparative data set to the globally applied WaterGAP 2 model. Comparisons to HYPE were used to judge our scaling approach, since HYPE simulations are readily available for the catchment associated with lake inflows, while measured lake inflow data are far less common.

While this study focuses exclusively on Swedish lakes, the wide range of topographic and geomorphological conditions represented in the datasets supports the potential global applicability of the scaling approach (Table S1). The dataset spans more than three orders of magnitude in lake surface area (from 0.34 to 5486 km$^2$) and are embedded in catchments ranging from 101 to 48421 km$^2$, with catchment-to-lake area ratios varying from 3.37 to 14962. These systems span a broad latitudinal gradient, from approximately 55°N to 69°N, encompassing temperate subarctic climates, and also cover a wide elevational range, from lowland lakes near sea level to high altitudes systems. This introduces variability in temperature regimes, snow accumulation and runoff dynamics. Catchment topography is similarly diverse, with mean catchment slopes ranging from 0.000001 to 0.012 m m$^{-1}$, and a wide spread in both minimum and maximum catchment slopes that influence flow concentration and hydrologic connectivity. This richness in latitude, elevation, slope, area and catchment configuration reflects a broad spectrum of geomorphic and hydrological settings. Since these land-based drivers are primary controls on surface hydrology and lake water balances, their strong representation in the Swedish dataset supports the scaling approach's transferability to other regions.

Although our scaling approach is effective for estimating how much water flows into lakes, it does not account for the full routing of water through rivers. A key limitation comes from differences in the spatial detail of the datasets we used. Water fluxes ($q_{tot}$, $q_g$ and $dis$) are provided by WaterGAP 2.2e on a coarse grid (0.5°grid cell), while geometry of lake boundaries in

the HydroLAKES dataset is represented at a much finer scale. This mismatch in resolution can lead to inconsistencies, for example: an inflowing stream might appear to flow into a lake in the gridded data, even though in reality it joins the river downstream. These issues are especially common in small lake systems. To reduce their impact, we used known catchment areas to adjust our streamflow estimates and avoid large overestimations. However, this approach does not fully resolve the

355 mismatches, and it breaks the water mass balance, meaning we may misrepresent how much water flows through the system. If the objective is to model the transport of water through river and lake networks, additional considerations would be required to ensure an accurate mass balance.

The task of linking ISIMIP Global Water Sector and Lake Sector models requires the use of gridded models and gridded data. One critical factor influencing the accuracy of the simulated streamflow is the structure and potential limitations of the gridded

360 hydrological model. In this study, the gridded water flux ($q_{tot}$, $q_g$ and $dis$) simulations were obtained from WaterGAP 2.2e (Müller Schmied et al., 2023), a global hydrological model that simulates water availability and use at a global scale. The performance of the scaling approach, when the simulated streamflow is compared to reference values or observations, is thus inherently linked to the accuracy of WaterGAP 2.2e outputs. The WaterGAP 2.2e model achieved a global monthly streamflow performance with a median *KGE* of 0.58 (Müller Schmied et al., 2023). The scaled streamflow simulations performed

365 similarly, with a median *KGE* of 0.59 compared to the reference and a median *KGE* of 0.46 against observations. Regarding *KGE* components, the bias ratio ($KGE_b$) showed a median value close to the optimal value of 1 in all cases (for WaterGAP 2.2e: median $KGE_b$ of 1.01 and for scaled streamflow: median $KGE_b$ of 1.04 compared to the reference and median $KGE_b$ of 1.00 compared to observations). $KGE_g$ deviates from 1, indicating that streamflow variability is not well simulated, the median $KGE_g$ was 0.86 for WaterGAP 2.2e, while the scaled streamflow showed median $KGE_g$ values of 0.84 compared to the

370 reference and 0.96 compared to observations. This underestimation of streamflow variability suggests that hydrological extremes, including peak and low flows, may not be fully captured when using a gridded model with gridded meteorological forcing, potentially leading to a smoothing effect in the simulations. In the Köppen-Geiger climate region D, which includes Sweden, 47 % of the gauging stations used for the calibration of WaterGAP 2.2e showed $KGE_g$ values between 0.5 and 0.9. For the scaled streamflow, 61 % of the study sites fell within 0.5-0.9 range when compared to the reference, while 40 % did

375 so when compared to observations. The ability to capture the timing of streamflow increases and decreases was generally good in WaterGAP 2.2e, with a median $KGE_r$ of 0.78. In the Köppen-Geiger climate region D, 27 % of gauging stations showed a $KGE_r$ below 0.5, indicating moderate timing errors. The scaled streamflow showed improved timing accuracy when compared to the reference, with a median $KGE_r$ of 0.81 and only 11% below 0.5. However, when compared to observations, the median $KGE_r$ decreases to 0.67, with 60% of study below 0.5, suggesting that while the scaling approach improves consistency with

380 the reference, discrepancies remain when validated against observed streamflow.

Another factor influencing the performance of streamflow simulations was the data source used for validation. E-HYPE, the European-scale implementation of the HYPE model, utilized gauged streamflow data for catchments larger than 5000 km$^2$, while for smaller catchments, it relies on modelled ungauged streamflow (Donnelly et al., 2016). This distinction is important because it might explain why the accuracy of streamflow simulations tended to be higher in well-gauged large catchments,

385      whereas streamflow simulations in smaller catchments were inherently more uncertain due to the reliance on hydrological modeling rather than observations. Among the 70 study sites, 23 had a catchment area larger than 5000 km$^2$, yielding a mean *KGE* of 0.60±0.22, while the remaining 47 study sites ($\leq$ 5000 km$^2$) exhibited a comparable performance, with a mean *KGE* of 0.58±0.15. However, for the 10 study sites where scaled streamflow was compared directly with observations, performance varied: 6 study sites with catchments larger than 5000 km$^2$ showed a mean *KGE* of 0.41±0.20, whereas another 4 study sites

390      ($\leq$ 5000 km$^2$) achieved a mean *KGE* of 0.52±0.22. This suggests that while scaled streamflow simulations performed similarly across different catchment sizes when compared to a streamflow reference, their accuracy was more variable when directly validated against observations.

     It is important to point out the difference between the reference (E-HYPE discharge simulations) and scaled streamflow are due not only to potential inaccuracies in the scaling approach itself, but also to differences in the performance of E-HYPE and

395      WaterGAP 2.2e models, and meteorological data used to force both models. The good agreement between the reference and simulated scaled streamflow, despite multiple potential sources of errors, therefore, suggests that the scaling approach presented here is likely to perform similarly well in another region of the world.

     When scaling streamflow from gridded data to the catchment scale, three different approaches (Approach I.a, Approach I.b and Approach II) were employed to account for differences in the size and location of lakes and their catchments in relation to

400      grid cells. These approaches are essential due to the significant differences in lake size, shape and catchment area relative to the model grid resolution. The performance of the scaling approach was further assessed across different catchment and lake sizes. For lakes where $A_{lake} \leq A_{grid}$, both sub-approaches (I.a and I.b) yielded similar results, demonstrating the robustness of the method across different grid configurations. In large lakes where $A_{lake} > A_{grid}$ (Approach II), such as Vänern and Vättern, the performance was strong with *KGE* values of 0.77 and 0.79, respectively. In contrast, for Lake Mälaren, which has a highly

405      irregular shape (Figure S1), the choice of scaling approach significantly affected performance. The better performance of Approach I.b (*KGE*=0.71) compared to Approach II (*KGE*=0.47) highlights the importance of accounting for complex lake morphologies in streamflow scaling. Nevertheless, both scaling approaches achieved satisfactory performance comparable to other lakes with less complex morphologies, indicates that, although lake morphology can influence performance, it is not the sole determining factor, further supporting the robustness and practical applicability of the scaling approaches even for lakes

410      with complex morphologies.

     Although validation against observed streamflow is constrained due to data availability, the 10 lakes used for validation are broadly representative of the 70 lakes included in the study. Geographically, these lakes are distributed across latitudes from 58.33° to 66.66°, covering southern, central and northern regions of Sweden (Table S3). The lake area spans three orders of magnitude from 7.68 km$^2$ (lake 142240) to 5486 km$^2$ (lake Vänern), with catchment areas that vary independently of lake size

415      ($A_{catchment}$ raged from 138.7 km$^2$ to 48421 km$^2$). This includes both small lakes with small catchments ($A_{catchment} A_{lake}^{-1}$ of 5.99 – lake Erken) and large catchments ($A_{catchment} A_{lake}^{-1}$ of 139.91– lake Roxen), as well as large lakes with small catchments ($A_{catchment} A_{lake}^{-1}$ of 3.37 – Lake Vättern) and large catchments ($A_{catchment} A_{lake}^{-1}$ of 20.94 – Lake Mälaren), reflecting the diverse hydrological characteristics of the study region. Validation against observed streamflow data for these representative lakes

(Figure 6B; Table S3) confirmed the ability of the scaled simulations to match not only reference data, but also observed data. Seasonal-scale performance was slightly lower (*KGE* of 0.46±0.21) due to timing errors, compared to stronger annual-scale performance (*KGE* of 0.70±0.15), indicating that the method effectively captures long-term hydrological trends.

## 5. Conclusion

The results of this study demonstrate that the developed scaling approach is reliable and robust for global applications, showing good performance across a wide range of hydrological settings. By implementing three distinct approaches (I.a, I.b and II), the methodology effectively accounts for varying lake sizes and catchment configurations, from small single-grid lakes and catchments to large, complex multi-grid systems such as Vänern, Vättern and Mälaren. This flexibility enables consistent application across diverse hydrological regimes and supports the use of the method in a large-scale modelling framework. While the overall performance was satisfactory, evidence by strong average *KGE* values, some limitations remain, particularly in capturing flow variability and timing in more complex systems.

This study also addresses a key limitation in the ISIMIP framework by introducing a method to dynamically link gridded catchment hydrology with lake inflows. The approach allows lake simulations to reflect not only direct climate impacts but also changes in upstream hydrological processes, enabling more realistic assessments of climate change impacts on lakes globally. By bridging the gap between catchment and lake dynamics, this methodology provides a valuable tool for improving integrated hydrological and biogeochemical lake modelling within ISIMIP and beyond.

## Acknowledgements

We are grateful to ISIMIP for producing, coordinating and making available the ISIMIP experiments. We also acknowledge the contribution of the ISIMIP Global Water Sector modelling teams for providing the hydrological simulations that formed the basis of this study. This research funding was supported by Vetenskapsrådet under project ID 2021-04639.

## Code availability

All R scripts produced during this study are available at https://doi.org/10.5281/zenodo.17589293 (Ayala, 2025a).

## Data availability

The impact model WaterGAP 2.2e simulations of monthly discharge (*dis*), total runoff ($q_{tot}$) and groundwater runoff ($q_g$) (Müller Schmied et al., 2024b) for the standard evaluation experiment *obsclim_histsoc_default* (Frieler et al., 2024), along with the drainage direction map and slopes for river routine, are available in the ISIMIP repository (https://data.isimip.org) and at https://doi.org/10.5281/zenodo.17588875 (Ayala, 2025b). Representative lakes at the ISIMIP3 Global Lake Sector can

be accessed at https://github.com/icra/ISIMIP_Lake_Sector. Scaled streamflow simulations for the 70 studied sites are available at https://doi.org/10.5281/zenodo.17588905 (Ayala, 2025c).

**Author contributions**

AIA led the study. AIA and JLH developed the scaled method with contributions from SNG, DCP and SS. AIA and JLH generated and validated the scaled streamflow data. AIA wrote the paper with contributions from JLH, DMB, RM, SNG, DCP and SS.

**Competing interests**

The contact author has declared that neither of the authors has any competing interests.

**References**

Alcamo, J., Döll, P., Henrichs, T., Kaspar, F., Lehner, B., Rösch, T., and Siebert, S.: Development and testing of the WaterGAP 2 global model of water use and availability, Hydrol. Sci. J., 48, 317–337, https://doi.org/10.1623/hysj.48.3.317.45290, 2003.

Ayala, A. I.: aiayalaz/Scaling-of-streamflow-inputs-to-lakes-ISIMIP3a: version 1.1.0 of Scaling of streamflow inputs to lakes ISIMIP3a (v1.1.0), https://doi.org/10.5281/ZENODO.17589293, 2025a.

Ayala, A. I.: Input data used in script scaling streamflow inputs to lakes in ISIMIP3a (Global Water-Lake Sector coupling), https://doi.org/10.5281/zenodo.17588875, 2025b.

Ayala, A. I.: Outputs from the script for scaling streamflow inputs to lakes in ISIMIP3a (Global Water–Lake Sector coupling), https://doi.org/10.5281/zenodo.17588905, 2025c.

Ayala, A. I., Moras, S., and Pierson, D. C.: Simulations of future changes in thermal structure of Lake Erken: proof of concept for ISIMIP2b lake sector local simulation strategy, Hydrol. Earth Syst. Sci., 24, 3311–3330, https://doi.org/10.5194/hess-24-3311-2020, 2020.

Ayala, A. I., Mesman, J. P., Jones, I. D., De Eyto, E., Jennings, E., Goyette, S., and Pierson, D. C.: Climate Change Impacts on Surface Heat Fluxes in a Deep Monomictic Lake, J. Geophys. Res. Atmospheres, 128, e2022JD038355, https://doi.org/10.1029/2022JD038355, 2023a.

Ayala, A. I., De Eyto, E., Jennings, E., Goyette, S., and Pierson, D. C.: Global warming will change the thermal structure of Lough Feeagh, a sentinel lake in the Irish landscape, by the end of the twenty-first century., Biol. Environ. Proc. R. Ir. Acad., 123B, 145–163, https://doi.org/10.1353/bae.2023.a916008, 2023b.

Costa, D., Sutter, C., Shepherd, A., Jarvie, H., Wilson, H., Elliott, J., Liu, J., and Macrae, M.: Impact of climate change on catchment nutrient dynamics: insights from around the world, Environ. Rev., 31, 4–25, https://doi.org/10.1139/er-2021-0109, 2023.

Cucchi, M., Weedon, G. P., Amici, A., Bellouin, N., Lange, S., Müller Schmied, H., Hersbach, H., and Buontempo, C.: WFDE5: bias-adjusted ERA5 reanalysis data for impact studies, Earth Syst. Sci. Data, 12, 2097–2120, https://doi.org/10.5194/essd-12-2097-2020, 2020.

480    Döll, P. and Lehner, B.: Validation of a new global 30-min drainage direction map, J. Hydrol., 258, 214–231, https://doi.org/10.1016/s0022-1694(01)00565-0, 2002.

Döll, P., Kaspar, F., and Lehner, B.: A global hydrological model for deriving water availability indicators: model tuning and validation, J. Hydrol., 270, 105–134, https://doi.org/10.1016/s0022-1694(02)00283-4, 2003.

Donnelly, C., Andersson, J. C. M., and Arheimer, B.: Using flow signatures and catchment similarities to evaluate the E-HYPE multi-basin model across Europe, https://doi.org/10.1080/02626667.2015.1027710, 2016.

485    Donnelly, C., Greuell, W., Andersson, J., Gerten, D., Pisacane, G., Roudier, P., and Ludwig, F.: Impacts of climate change on European hydrology at 1.5, 2 and 3 degrees mean global warming above preindustrial level, Clim. Change, 143, 13–26, https://doi.org/10.1007/s10584-017-1971-7, 2017.

Fenocchi, A., Rogora, M., Sibilla, S., and Dresti, C.: Relevance of inflows on the thermodynamic structure and on the modeling of a deep subalpine lake (Lake Maggiore, Northern Italy/Southern Switzerland), Limnologica, 63, 42–56, https://doi.org/10.1016/j.limno.2017.01.006, 2017.

490

Frieler, K., Volkholz, J., Lange, S., Schewe, J., Mengel, M., Rivas López, M. D. R., Otto, C., Reyer, C. P. O., Karger, D. N., Malle, J. T., Treu, S., Menz, C., Blanchard, J. L., Harrison, C. S., Petrik, C. M., Eddy, T. D., Ortega-Cisneros, K., Novaglio, C., Rousseau, Y., Watson, R. A., Stock, C., Liu, X., Heneghan, R., Tittensor, D., Maury, O., Büchner, M., Vogt, T., Wang, T., Sun, F., Sauer, I. J., Koch, J., Vanderkelen, I., Jägermeyr, J., Müller, C., Klar, J., Vega Del Valle, 495    I. D., Lasslop, G., Chadburn, S., Burke, E., Gallego-Sala, A., Smith, N., Chang, J., Hantson, S., Burton, C., Gädeke, A., Li, F., Gosling, S. N., Müller Schmied, H., Hattermann, F., Wang, J., Yao, F., Hickler, T., Marcé, R., Pierson, D., Thiery, W., Mercado-Bettín, D., Forrest, M., and Bechtold, M.: Scenario set-up and forcing data for impact model evaluation and impact attribution within the third round of the Inter-Sectoral Model Intercomparison Project (ISIMIP3a), Geosci. Model Dev., 17, 1–51, https://doi.org/10.5194/gmd-17-1-2024, 2024.

500    Golub, M., Thiery, W., Marcé, R., Pierson, D., Vanderkelen, I., Mercado-Bettin, D., Woolway, R. I., Grant, L., Jennings, E., Kraemer, B. M., Schewe, J., Zhao, F., Frieler, K., Mengel, M., Bogomolov, V. Y., Bouffard, D., Côté, M., Couture, R.-M., Debolskiy, A. V., Droppers, B., Gal, G., Guo, M., Janssen, A. B. G., Kirillin, G., Ladwig, R., Magee, M., Moore, T., Perroud, M., Piccolroaz, S., Raaman Vinnaa, L., Schmid, M., Shatwell, T., Stepanenko, V. M., Tan, Z., Woodward, B., Yao, H., Adrian, R., Allan, M., Anneville, O., Arvola, L., Atkins, K., Boegman, L., Carey, C., 505    Christianson, K., De Eyto, E., DeGasperi, C., Grechushnikova, M., Hejzlar, J., Joehnk, K., Jones, I. D., Laas, A., Mackay, E. B., Mammarella, I., Markensten, H., McBride, C., Özkundakci, D., Potes, M., Rinke, K., Robertson, D., Rusak, J. A., Salgado, R., Van Der Linden, L., Verburg, P., Wain, D., Ward, N. K., Wollrab, S., and Zdorovennova, G.: A framework for ensemble modelling of climate change impacts on lakes worldwide: the ISIMIP Lake Sector, Geosci. Model Dev., 15, 4597–4623, https://doi.org/10.5194/gmd-15-4597-2022, 2022.

510    Grant, L., Vanderkelen, I., Gudmundsson, L., Tan, Z., Perroud, M., Stepanenko, V. M., Debolskiy, A. V., Droppers, B., Janssen, A. B. G., Woolway, R. I., Choulga, M., Balsamo, G., Kirillin, G., Schewe, J., Zhao, F., Del Valle, I. V., Golub, M., Pierson, D., Marcé, R., Seneviratne, S. I., and Thiery, W.: Attribution of global lake systems change to anthropogenic forcing, Nat. Geosci., 14, 849–854, https://doi.org/10.1038/s41561-021-00833-x, 2021.

Gronchi, E., Jöhnk, K. D., Straile, D., Diehl, S., and Peeters, F.: Local and continental-scale controls of the onset of spring 515    phytoplankton blooms: Conclusions from a proxy-based model, Glob. Change Biol., 27, 1976–1990, https://doi.org/10.1111/gcb.15521, 2021.

Gupta, H. V., Kling, H., Yilmaz, K. K., and Martinez, G. F.: Decomposition of the mean squared error and NSE performance criteria: Implications for improving hydrological modelling, J. Hydrol., 377, 80–91, https://doi.org/10.1016/j.jhydrol.2009.08.003, 2009.

520 Huisman, J., Codd, G. A., Paerl, H. W., Ibelings, B. W., Verspagen, J. M. H., and Visser, P. M.: Cyanobacterial blooms, Nat. Rev. Microbiol., 16, 471–483, https://doi.org/10.1038/s41579-018-0040-1, 2018.

Jane, S. F., Hansen, G. J. A., Kraemer, B. M., Leavitt, P. R., Mincer, J. L., North, R. L., Pilla, R. M., Stetler, J. T., Williamson, C. E., Woolway, R. I., Arvola, L., Chandra, S., DeGasperi, C. L., Diemer, L., Dunalska, J., Erina, O., Flaim, G., Grossart, H.-P., Hambright, K. D., Hein, C., Hejzlar, J., Janus, L. L., Jenny, J.-P., Jones, J. R., Knoll, L. B., Leoni, 525 B., Mackay, E., Matsuzaki, S.-I. S., McBride, C., Müller-Navarra, D. C., Paterson, A. M., Pierson, D., Rogora, M., Rusak, J. A., Sadro, S., Saulnier-Talbot, E., Schmid, M., Sommaruga, R., Thiery, W., Verburg, P., Weathers, K. C., Weyhenmeyer, G. A., Yokota, K., and Rose, K. C.: Widespread deoxygenation of temperate lakes, Nature, 594, 66–70, https://doi.org/10.1038/s41586-021-03550-y, 2021.

Jansen, J., Woolway, R. I., Kraemer, B. M., Albergel, C., Bastviken, D., Weyhenmeyer, G. A., Marcé, R., Sharma, S., Sobek, 530 S., Tranvik, L. J., Perroud, M., Golub, M., Moore, T. N., Råman Vinnå, L., La Fuente, S., Grant, L., Pierson, D. C., Thiery, W., and Jennings, E.: Global increase in methane production under future warming of lake bottom waters, Glob. Change Biol., 28, 5427–5440, https://doi.org/10.1111/gcb.16298, 2022.

Jansen, J., Simpson, G. L., Weyhenmeyer, G. A., Härkönen, L. H., Paterson, A. M., Del Giorgio, P. A., and Prairie, Y. T.: Climate-driven deoxygenation of northern lakes, Nat. Clim. Change, 14, 832–838, https://doi.org/10.1038/s41558-535 024-02058-3, 2024.

Jiménez-Navarro, I. C., Jimeno-Sáez, P., López-Ballesteros, A., Pérez-Sánchez, J., and Senent-Aparicio, J.: Impact of Climate Change on the Hydrology of the Forested Watershed That Drains to Lake Erken in Sweden: An Analysis Using SWAT+ and CMIP6 Scenarios, Forests, 12, 1803, https://doi.org/10.3390/f12121803, 2021.

Jones, E. R., Van Beek, R., Cárdenas Belleza, G., Burek, P., Dugdale, S. J., Flörke, M., Fridman, D., Gosling, S. N., Kumar, 540 R., Mercado-Bettin, D., Müller Schmied, H., Tan, Z., Thiery, W., Tilahun, A. B., Wanders, N., and Van Vliet, M. T. H.: A multi-model assessment of global freshwater temperature and thermoelectric power supply under climate change, Environ. Res. Water, 1, 025002, https://doi.org/10.1088/3033-4942/addffa, 2025.

Kim, H.: Global Soil Wetness Project Phase 3 Atmospheric Boundary Conditions (Experiment 1), https://doi.org/10.20783/DIAS.501, 2017.

545 Kling, H., Fuchs, M., and Paulin, M.: Runoff conditions in the upper Danube basin under an ensemble of climate change scenarios, J. Hydrol., 424–425, 264–277, https://doi.org/10.1016/j.jhydrol.2012.01.011, 2012.

Knoben, W. J. M., Freer, J. E., and Woods, R. A.: Technical note: Inherent benchmark or not? Comparing Nash–Sutcliffe and Kling–Gupta efficiency scores, Hydrol. Earth Syst. Sci., 23, 4323–4331, https://doi.org/10.5194/hess-23-4323-2019, 2019.

550 Kraemer, B. M., Anneville, O., Chandra, S., Dix, M., Kuusisto, E., Livingstone, D. M., Rimmer, A., Schladow, S. G., Silow, E., Sitoki, L. M., Tamatamah, R., Vadeboncoeur, Y., and McIntyre, P. B.: Morphometry and average temperature affect lake stratification responses to climate change, Geophys. Res. Lett., 42, 4981–4988, https://doi.org/10.1002/2015GL064097, 2015.

Krysanova, V., Vetter, T., Eisner, S., Huang, S., Pechlivanidis, I., Strauch, M., Gelfan, A., Kumar, R., Aich, V., Arheimer, B., 555 Chamorro, A., Van Griensven, A., Kundu, D., Lobanova, A., Mishra, V., Plötner, S., Reinhardt, J., Seidou, O., Wang,

X., Wortmann, M., Zeng, X., and Hattermann, F. F.: Intercomparison of regional-scale hydrological models and climate change impacts projected for 12 large river basins worldwide—a synthesis, Environ. Res. Lett., 12, 105002, https://doi.org/10.1088/1748-9326/aa8359, 2017.

560 La Fuente, S., Jennings, E., Gal, G., Kirillin, G., Shatwell, T., Ladwig, R., Moore, T., Couture, R.-M., Côté, M., Love Råman Vinnå, C., and Iestyn Woolway, R.: Multi-model projections of future evaporation in a sub-tropical lake, J. Hydrol., 615, 128729, https://doi.org/10.1016/j.jhydrol.2022.128729, 2022.

La Fuente, S., Jennings, E., Lenters, J. D., Verburg, P., Tan, Z., Perroud, M., Janssen, A. B. G., and Woolway, R. I.: Ensemble modeling of global lake evaporation under climate change, J. Hydrol., 631, 130647, https://doi.org/10.1016/j.jhydrol.2024.130647, 2024a.

565 La Fuente, S., Jennings, E., Lenters, J. D., Verburg, P., Kirillin, G., Shatwell, T., Couture, R.-M., Côté, M., Vinnå, C. L. R., and Woolway, R. I.: Increasing warm-season evaporation rates across European lakes under climate change, Clim. Change, 177, 173, https://doi.org/10.1007/s10584-024-03830-2, 2024b.

Lange, S., Volkholz, J., Geiger, T., Zhao, F., Vega, I., Veldkamp, T., Reyer, C. P. O., Warszawski, L., Huber, V., Jägermeyr, J., Schewe, J., Bresch, D. N., Büchner, M., Chang, J., Ciais, P., Dury, M., Emanuel, K., Folberth, C., Gerten, D., 570 Gosling, S. N., Grillakis, M., Hanasaki, N., Henrot, A., Hickler, T., Honda, Y., Ito, A., Khabarov, N., Koutroulis, A., Liu, W., Müller, C., Nishina, K., Ostberg, S., Müller Schmied, H., Seneviratne, S. I., Stacke, T., Steinkamp, J., Thiery, W., Wada, Y., Willner, S., Yang, H., Yoshikawa, M., Yue, C., and Frieler, K.: Projecting Exposure to Extreme Climate Impact Events Across Six Event Categories and Three Spatial Scales, Earths Future, 8, e2020EF001616, https://doi.org/10.1029/2020EF001616, 2020.

575 Lange, S., Menz, C., Gleixner, S., Cucchi, M., Weedon, G. P., Amici, A., Bellouin, N., Müller Schmied, Hans Hersbach, Buontempo, C., and Cagnazzo, C.: WFDE5 over land merged with ERA5 over the ocean (W5E5 v2.0), https://doi.org/10.48364/ISIMIP.342217, 2021.

Li, X., Peng, S., Xi, Y., Woolway, R. I., and Liu, G.: Earlier ice loss accelerates lake warming in the Northern Hemisphere, Nat. Commun., 13, 5156, https://doi.org/10.1038/s41467-022-32830-y, 2022.

580 Lindström, G., Pers, C., Rosberg, J., Strömqvist, J., and Arheimer, B.: Development and testing of the HYPE (Hydrological Predictions for the Environment) water quality model for different spatial scales, Hydrol. Res., 41, 295–319, https://doi.org/10.2166/nh.2010.007, 2010.

Liu, J., You, Y., Li, J., Sitch, S., Gu, X., Nabel, J. E. M. S., Lombardozzi, D., Luo, M., Feng, X., Arneth, A., Jain, A. K., Friedlingstein, P., Tian, H., Poulter, B., and Kong, D.: Response of global land evapotranspiration to climate change, 585 elevated $CO_2$, and land use change, Agric. For. Meteorol., 311, 108663, https://doi.org/10.1016/j.agrformet.2021.108663, 2021.

Maberly, S. C., O'Donnell, R. A., Woolway, R. I., Cutler, M. E. J., Gong, M., Jones, I. D., Merchant, C. J., Miller, C. A., Politi, E., Scott, E. M., Thackeray, S. J., and Tyler, A. N.: Global lake thermal regions shift under climate change, Nat. Commun., 11, 1232, https://doi.org/10.1038/s41467-020-15108-z, 2020.

590 Magee, M. R. and Wu, C. H.: Response of water temperatures and stratification to changing climate in three lakes with different morphometry, Hydrol. Earth Syst. Sci., 21, 6253–6274, https://doi.org/10.5194/hess-21-6253-2017, 2017.

Marotta, H., Pinho, L., Gudasz, C., Bastviken, D., Tranvik, L. J., and Enrich-Prast, A.: Greenhouse gas production in low-latitude lake sediments responds strongly to warming, Nat. Clim. Change, 4, 467–470, https://doi.org/10.1038/nclimate2222, 2014.

595   Mesman, J. P., Jiménez-Navarro, I. C., Ayala, A. I., Senent-Aparicio, J., Trolle, D., and Pierson, D. C.: Timing of spring events changes under modelled future climate scenarios in a mesotrophic lake, Hydrol. Earth Syst. Sci., 28, 1791–1802, https://doi.org/10.5194/hess-28-1791-2024, 2024.

Messager, M. L., Lehner, B., Grill, G., Nedeva, I., and Schmitt, O.: Estimating the volume and age of water stored in global lakes using a geo-statistical approach, Nat. Commun., 7, 13603, https://doi.org/10.1038/ncomms13603, 2016.

600   Moras, S., Ayala, A. I., and Pierson, D. C.: Historical modelling of changes in Lake Erken thermal conditions, Hydrol. Earth Syst. Sci., 23, 5001–5016, https://doi.org/10.5194/hess-23-5001-2019, 2019.

Müller Schmied, H., Cáceres, D., Eisner, S., Flörke, M., Herbert, C., Niemann, C., Peiris, T. A., Popat, E., Portmann, F. T., Reinecke, R., Schumacher, M., Shadkam, S., Telteu, C.-E., Trautmann, T., and Döll, P.: The global water resources and use model WaterGAP v2.2d: model description and evaluation, Geosci. Model Dev., 14, 1037–1079,
605   https://doi.org/10.5194/gmd-14-1037-2021, 2021.

Müller Schmied, H., Trautmann, T., Ackermann, S., Cáceres, D., Flörke, M., Gerdener, H., Kynast, E., Peiris, T. A., Schiebener, L., Schumacher, M., and Döll, P.: The global water resources and use model WaterGAP v2.2e: description and evaluation of modifications and new features, https://doi.org/10.5194/gmd-2023-213, 20 November 2023.

610   Müller Schmied, H., Gosling, S. N., Garnsworthy, M., Müller, L., Telteu, C.-E., Ahmed, A. K., Andersen, L. S., Boulange, J., Burek, P., Chang, J., Chen, H., Grillakis, M., Guillaumot, L., Hanasaki, N., Koutroulis, A., Kumar, R., Leng, G., Liu, J., Liu, X., Menke, I., Mishra, V., Pokhrel, Y., Rakovec, O., Samaniego, L., Satoh, Y., Shah, H. L., Smilovic, M., Stacke, T., Sutanudjaja, E., Thiery, W., Tsilimigkras, A., Wada, Y., Wanders, N., and Yokohata, T.: Graphical representation of global water models, https://doi.org/10.5194/egusphere-2024-1303, 6 May 2024a.

615   Müller Schmied, H., Trautmann, T., Ackermann, S., Cáceres, D., Flörke, M., Gerdener, H., Kynast, E., Peiris, T. A., Schiebener, L., Schumacher, M., and Döll, P.: The global water resources and use model WaterGAP v2.2e: description and evaluation of modifications and new features, Geosci. Model Dev., 17, 8817–8852, https://doi.org/10.5194/gmd-17-8817-2024, 2024b.

Nash, J. E. and Sutcliffe, J. V.: River flow forecasting through conceptual models part I — A discussion of principles, J.
620   Hydrol., 10, 282–290, https://doi.org/10.1016/0022-1694(70)90255-6, 1970.

North, R. P., North, R. L., Livingstone, D. M., Köster, O., and Kipfer, R.: Long-term changes in hypoxia and soluble reactive phosphorus in the hypolimnion of a large temperate lake: consequences of a climate regime shift, Glob. Change Biol., 20, 811–823, https://doi.org/10.1111/gcb.12371, 2014.

O'Reilly, C. M., Sharma, S., Gray, D. K., Hampton, S. E., Read, J. S., Rowley, R. J., Schneider, P., Lenters, J. D., McIntyre,
625   P. B., Kraemer, B. M., Weyhenmeyer, G. A., Straile, D., Dong, B., Adrian, R., Allan, M. G., Anneville, O., Arvola, L., Austin, J., Bailey, J. L., Baron, J. S., Brookes, J. D., De Eyto, E., Dokulil, M. T., Hamilton, D. P., Havens, K., Hetherington, A. L., Higgins, S. N., Hook, S., Izmest'eva, L. R., Joehnk, K. D., Kangur, K., Kasprzak, P., Kumagai, M., Kuusisto, E., Leshkevich, G., Livingstone, D. M., MacIntyre, S., May, L., Melack, J. M., Mueller-Navarra, D. C., Naumenko, M., Noges, P., Noges, T., North, R. P., Plisnier, P., Rigosi, A., Rimmer, A., Rogora, M., Rudstam, L.
630   G., Rusak, J. A., Salmaso, N., Samal, N. R., Schindler, D. E., Schladow, S. G., Schmid, M., Schmidt, S. R., Silow, E., Soylu, M. E., Teubner, K., Verburg, P., Voutilainen, A., Watkinson, A., Williamson, C. E., and Zhang, G.: Rapid and highly variable warming of lake surface waters around the globe, Geophys. Res. Lett., 42, https://doi.org/10.1002/2015GL066235, 2015.

Paerl, H. W. and Huisman, J.: Blooms Like It Hot, Science, 320, 57–58, https://doi.org/10.1126/science.1155398, 2008.

Råman Vinnå, L., Wüest, A., Zappa, M., Fink, G., and Bouffard, D.: Tributaries affect the thermal response of lakes to climate change, Hydrol. Earth Syst. Sci., 22, 31–51, https://doi.org/10.5194/hess-22-31-2018, 2018.

Rosenzweig, C., Arnell, N. W., Ebi, K. L., Lotze-Campen, H., Raes, F., Rapley, C., Smith, M. S., Cramer, W., Frieler, K., Reyer, C. P. O., Schewe, J., Van Vuuren, D., and Warszawski, L.: Assessing inter-sectoral climate change risks: the role of ISIMIP, Environ. Res. Lett., 12, 010301, https://doi.org/10.1088/1748-9326/12/1/010301, 2017.

Saber, A., James, D. E., and Hannoun, I. A.: Effects of lake water level fluctuation due to drought and extreme winter precipitation on mixing and water quality of an alpine lake, Case Study: Lake Arrowhead, California, Sci. Total Environ., 714, 136762, https://doi.org/10.1016/j.scitotenv.2020.136762, 2020.

Sharma, S., Blagrave, K., Magnuson, J. J., O'Reilly, C. M., Oliver, S., Batt, R. D., Magee, M. R., Straile, D., Weyhenmeyer, G. A., Winslow, L., and Woolway, R. I.: Widespread loss of lake ice around the Northern Hemisphere in a warming world, Nat. Clim. Change, 9, 227–231, https://doi.org/10.1038/s41558-018-0393-5, 2019.

Sharma, S., Richardson, D. C., Woolway, R. I., Imrit, M. A., Bouffard, D., Blagrave, K., Daly, J., Filazzola, A., Granin, N., Korhonen, J., Magnuson, J., Marszelewski, W., Matsuzaki, S. S., Perry, W., Robertson, D. M., Rudstam, L. G., Weyhenmeyer, G. A., and Yao, H.: Loss of Ice Cover, Shifting Phenology, and More Extreme Events in Northern Hemisphere Lakes, J. Geophys. Res. Biogeosciences, 126, e2021JG006348, https://doi.org/10.1029/2021JG006348, 2021.

Telteu, C.-E., Müller Schmied, H., Thiery, W., Leng, G., Burek, P., Liu, X., Boulange, J. E. S., Andersen, L. S., Grillakis, M., Gosling, S. N., Satoh, Y., Rakovec, O., Stacke, T., Chang, J., Wanders, N., Shah, H. L., Trautmann, T., Mao, G., Hanasaki, N., Koutroulis, A., Pokhrel, Y., Samaniego, L., Wada, Y., Mishra, V., Liu, J., Döll, P., Zhao, F., Gädeke, A., Rabin, S. S., and Herz, F.: Understanding each other's models: an introduction and a standard representation of 16 global water models to support intercomparison, improvement, and communication, Geosci. Model Dev., 14, 3843–3878, https://doi.org/10.5194/gmd-14-3843-2021, 2021.

Vachon, D., Langenegger, T., Donis, D., and McGinnis, D. F.: Influence of water column stratification and mixing patterns on the fate of methane produced in deep sediments of a small eutrophic lake, Limnol. Oceanogr., 64, 2114–2128, https://doi.org/10.1002/lno.11172, 2019.

Vanderkelen, I., Van Lipzig, N. P. M., Lawrence, D. M., Droppers, B., Golub, M., Gosling, S. N., Janssen, A. B. G., Marcé, R., Schmied, H. M., Perroud, M., Pierson, D., Pokhrel, Y., Satoh, Y., Schewe, J., Seneviratne, S. I., Stepanenko, V. M., Tan, Z., Woolway, R. I., and Thiery, W.: Global Heat Uptake by Inland Waters, Geophys. Res. Lett., 47, e2020GL087867, https://doi.org/10.1029/2020GL087867, 2020.

Wang, W., Lee, X., Xiao, W., Liu, S., Schultz, N., Wang, Y., Zhang, M., and Zhao, L.: Global lake evaporation accelerated by changes in surface energy allocation in a warmer climate, Nat. Geosci., 11, 410–414, https://doi.org/10.1038/s41561-018-0114-8, 2018.

Woolway, R. I. and Merchant, C. J.: Worldwide alteration of lake mixing regimes in response to climate change, Nat. Geosci., 12, 271–276, https://doi.org/10.1038/s41561-019-0322-x, 2019.

Woolway, R. I., Jennings, E., Shatwell, T., Golub, M., Pierson, D. C., and Maberly, S. C.: Lake heatwaves under climate change, Nature, 589, 402–407, https://doi.org/10.1038/s41586-020-03119-1, 2021a.

Woolway, R. I., Sharma, S., Weyhenmeyer, G. A., Debolskiy, A., Golub, M., Mercado-Bettín, D., Perroud, M., Stepanenko, V., Tan, Z., Grant, L., Ladwig, R., Mesman, J., Moore, T. N., Shatwell, T., Vanderkelen, I., Austin, J. A., DeGasperi, C. L., Dokulil, M., La Fuente, S., Mackay, E. B., Schladow, S. G., Watanabe, S., Marcé, R., Pierson, D. C., Thiery,

W., and Jennings, E.: Phenological shifts in lake stratification under climate change, Nat. Commun., 12, 2318, https://doi.org/10.1038/s41467-021-22657-4, 2021b.

Woolway, R. I., Albergel, C., Frölicher, T. L., and Perroud, M.: Severe Lake Heatwaves Attributable to Human-Induced Global Warming, Geophys. Res. Lett., 49, e2021GL097031, https://doi.org/10.1029/2021GL097031, 2022a.

Woolway, R. I., Denfeld, B., Tan, Z., Jansen, J., Weyhenmeyer, G. A., and La Fuente, S.: Winter inverse lake stratification under historic and future climate change, Limnol. Oceanogr. Lett., 7, 302–311, https://doi.org/10.1002/lol2.10231, 2022b.